Journal of Power Sources 268 (2014) 69–76

Contents lists available at ScienceDirect

Journal of Power Sources

journal homepage: www.elsevier.com/locate/jpowsour

Oxygen evolution in Co-doped RuO_2 and IrO_2: Experimental and theoretical insights to diminish electrolysis overpotential

R.G. González-Huerta [a], G. Ramos-Sánchez [b], P.B. Balbuena [b, *]

[a] Instituto Politécnico Nacional-ESIQIE, Laboratorio Electroquímica y Corrosión, UPALM, CP 07738 México D.F., Mexico
[b] Artie Mc. Ferrin Department of Chemical Engineering, Texas A&M University, College Station, TX 77843, USA

HIGHLIGHTS

- At low over-potential current densities $RuIrCoO_x$ shows the lowest Tafel slope value, 0.068 V dec^{-1}.
- The experimental Tafel slope suggests that OH dissociation should be the rate-determining step.
- DFT calculations show that the second OH bond breaking has a higher barrier than the first one.
- Doping with Co allows higher driving force and a small activation barrier.

ARTICLE INFO

Article history:
Received 4 March 2014
Received in revised form
5 June 2014
Accepted 5 June 2014
Available online 13 June 2014

Keywords:
Density functional theory
Doped oxides
Oxygen evolution reaction
Electrocatalysis

ABSTRACT

Development of proton exchange membrane (PEM) water electrolysis systems has been held back by the cost of membrane and precious metal electrocatalyst components, and by the high overvoltage for water splitting. Since non-noble metal electrocatalysts with satisfactory activities are not currently available, costs must be reduced by improving performance and durability of noble metal electrocatalysts. Moreover, it is mandatory to understand the mechanisms of oxygen evolution and find out how the reaction kinetics could be improved. Here the kinetic pathway for oxygen evolution reaction (OER) on RuO_2, IrO_2 and $RuIrCoO_x$ surfaces is analyzed with electrochemical polarization and Density Functional Theory (DFT) analyses of the changes occurring when pure oxides are doped with Co and their effect during the first stages of oxygen evolution. Experimental electrochemical methods are used to find indicators of electrocatalyst quality: the lower the Tafel slope, the faster the reaction kinetics and the more active the electrocatalyst. It is found that $RuIrCoO_x$ surfaces show the lowest Tafel slope value, 0.068 V dec^{-1}, and the rate determining step at low overpotential is the second H–O breaking. Changes in electronic structure responsible of the sluggish second reduction step in comparison to the first are identified by the theoretical study.

1. Introduction

Electrodes for PEM electrolysis should possess many desirable characteristics such as high stability, low cost and the lowest possible overpotential for the Oxygen Evolution Reaction. Among the different options, transition metal oxides have specific properties that can be modified in order to made them suitable for a vast range of applications: chemical nature of the oxide, morphology (dispersed state, crystal size, crystallinity, etc.), nonstoichiometric characteristics (ionic defects, electronic defects, solid state redox properties, etc.), magnetic properties, band structure of the oxide, surface electronic structure, geometric factors, crystal-field stabilization energy and synergistic effects (mixed and doped oxides). Many metal oxides show poor stability at anodic potentials of the OER; moreover, most of the overpotential losses during electrochemical hydrogen production are related to the electrochemical processes at the anode, where the OER takes place. Several studies have shown that noble metal oxides, such as iridium oxide (IrO_2) and ruthenium oxide (RuO_2), exhibit good OER performance [1–4]. Although RuO_2 is known to be a highly active electrocatalyst it lacks long term stability [5]. On the other hand, IrO_2 is a preferred material because of its higher stability but its activity must be further improved to lower the specific electric power consumption [6].

* Corresponding author. 3122 TAMU, College Station, TX 77843, USA. Tel.: +1 979 845 3375.
E-mail address: balbuena@tamu.edu (P.B. Balbuena).

http://dx.doi.org/10.1016/j.jpowsour.2014.06.029
0378-7753/

Another route is to form mixtures of RuO_2/IrO_2, mixing non-precious metals having dissimilar electronic character induces pronounced synergetic effects on electrocatalytic activity, which has been previously reported to have a significant improvement in the catalytic activity [7]. Although it has been recognized that the use of mixed metals can lead to synergetic effects that could improve the kinetics for the OER and the stability/selectivity of the oxygen electrode, modern electrocatalysis trends tend to reduce or completely replace precious metals in the catalyst while keeping the same level of efficiency. Hence, two viable routes to address the cost saving/enhancing activity issue behind the development of new non-noble electrocatalysts are: 1) forming bimetallic catalysts and 2) adding a dopant such as SnO_2, TiO_2, Co_3O_4, etc., to obtain a material with both high activity and stability so that the anode electrocatalyst loading can be reduced [4,7,8]. For example, Co is a transition element with incomplete electron shell that has shown interesting catalytic properties as component of electrocatalysts for the Oxygen Reduction Reaction (ORR) in acid medium, but the catalytic activity of metallic cobalt in PEM water electrolyzer was reported as poor due to its instability in acid media. So, further research is oriented to electrocatalysts with mixed phases containing cobalt oxides, such as Co_3O_4 that has been shown as a promoter for reducing noble metal components in catalysts for fuel cells [9]. In this work an anodic electrocatalyst $IrRuCoO_x$ is prepared by chemical reduction. Its synthesis, physical and electrochemical characterization were reported previously [1]. Here we discuss the kinetic pathway and a theoretical study of the OER on $IrRuCoO_x$ surfaces. The effect of dopants on the overall OER mechanism and kinetics is investigated by a molecular modeling approach.

2. Methodology

2.1. Experimental procedure

As described previously [1], nanometric $IrRuCo_x$ catalysts have been synthesized by a chemical reduction method using $CoCl_2$, $RuCl_3 \cdot H_2O$, and $IrCl_3 \cdot H_2O$ as precursors. Briefly, these precursors were diluted in tetrahydrofuran (99%) in order to prepare an atomic ratio IrRuCo 1:1:1. The solution was then heated (60 °C) under air atmosphere and magnetically stirred for 30 min; $NaBH_4$ was added as a reducing agent. The reaction products were washed with distilled water and filtered. After filtration, the powder was dried and weighted thus obtaining a 95% yield. In order to obtain the oxides, the compound was subjected to thermal treatment in an air atmosphere at 450 °C, in a temperature-controlled MTI model GSL-1100X furnace at 4 °C min^{-1} for 3 h. Thereafter, the resultant powder was maintained in a closed vessel located inside desiccators. Two extra samples of pure RuO_2 and IrO_2 catalysts were prepared by the same chemical method for comparison purposes.

The kinetic behavior of the $RuIrCoO_x$ catalysts for the OER was analyzed by linear voltammetry experiments. A solution (60 mL of ethanol and 5 mL of Nafion® and 60 mL of water) of catalyst (1 mg) was prepared and mixed in an ultrasonic bath. 8 mL of aqueous solution of catalyst were deposited on a glassy carbon substrate. Electrochemical analyses were carried out at room temperature in a conventional three-electrode cell consisting of the $RuIrCoO_x$ sample (working electrode), a reference electrode ($Hg/HgSO_4$ sat. 0.68 V vs NHE) and a platinum grid (counter electrode). The electrolyte solution was 0.5 M H_2SO_4. An inert gas was fed to the solution for 10 min before every test. The cell was connected to a Potentiostat/Galvanostat 263A (EG&G PAR) and PC (software EG&G Princeton Applied Research, PowerSuite 2.56, PowerSuit library 2.43.0). Linear voltammetry experiments were carried out from 1.23 to 1.68 V/NHE (Normal Hydrogen Electrode) at 20 mV s^{-1} scan rates in a rotating disk electrode at 900 rpm; each experiment was repeated 250 times at the same conditions to evaluate the catalysts stability. Initial cyclic voltammetric experiments were used to activate and eliminate residual synthesis products in a nitrogen degassed solution, by scanning in the range 1.23–1.68 V/NHE at 20 mV s^{-1} for 40 cycles.

2.2. Computational details

Plane-wave DFT as implemented in the Vienna ab Initio Simulation Package (VASP) [10,11] was used to perform all calculations employing the projector augmented wave (PAW) pseudopotentials [12,13]. The electron-exchange correlation was treated within the spin polarized general gradient approximation and the Revised Perdew–Becke–Ernzerhoff (RPBE) exchange correlation functional [14]. A quasi-Newton algorithm was used to relax ions into their instantaneous ground state, the atoms were allowed to relax but the cell and its shape were kept constant. The tetrahedron method with Bloch corrections was used to represent partial occupancies and a conjugate gradient algorithm was used for electronic minimization. The criteria for ionic and electronic convergence were set to 10^{-4} and 10^{-5} eV respectively for the difference between successive optimization steps. RuO_2 and IrO_2 bulk structures were fully optimized using the RPBE functional; the agreement between experimental and calculated lattice constants is within the 1% which confirms the adequateness of the simulated structure. The (110) surface was used for slab calculations, a 5-layer slab model was constructed; the two bottom layers were fixed and the three top layers were allowed to move during relaxations. Both Ir and Ru oxide (RuO_2 and IrO_2) crystallize in the tetragonal rutile structure; they are electrical conductors and present very similar properties. The (110) oriented domain is one of the dominant surfaces [15,16]. In the bulk structure metal atoms are coordinated to six oxygen atoms forming a slightly distorted octahedron (d^2sp^3 hybridization). When the (110) surface is formed two types of O atoms are formed: bridging O atoms above the surface which are coordinated to two metal atoms and three-coordinated atoms on the same plane of the metal atoms. The metallic atoms are penta-coordinated and hexa-coordinated atoms below the bridging atoms (Fig. 1a, b). The size of the slab is 1×2 to have two penta-coordinated metallic atoms and two hexa-coordinated atoms, thus two oxygen atoms of each type. A vacuum space is allowed between slabs in the z direction to avoid artificial interactions. Doping with Co was allowed in the surface in both metallic sites, the addition of Co forms different adsorption sites depending on the site of doping.

3. Results

3.1. Kinetic pathway analysis

Linear voltammetry curves are shown in Fig. 2 for the pure and doped oxides. The pure IrO_2 material shows an onset potential for oxygen evolution at 1.5 V; the current density obtained in the IrO_2 electrode (34 mA cm^{-2}) is higher than that in $RuIrCoO_x$ catalysts (22 mA cm^{-2}) at 1.68 V, and the lowest current density is showed by RuO_2 electrode (only 10 mA cm^{-2}). However the $RuIrCoO_x$ catalyst is more stable in the reaction medium than both RuO_2 and IrO_2 catalysts, since the linear voltamperogram of the $RuIrCoO_x$ electrode are easily reproduced whereas on RuO_2 and IrO_2 electrodes the current density decreased in each cycle. Moreover, additional experiments were performed up to 250 cycles (Supplementary information Fig. S1) in which the voltammograms obtained with $RuIrCo_x$ remain stable while the voltammograms on IrO_2 show slight stability decrease with time and those on RuO_2 present increasingly higher current density decrease at each cycle.

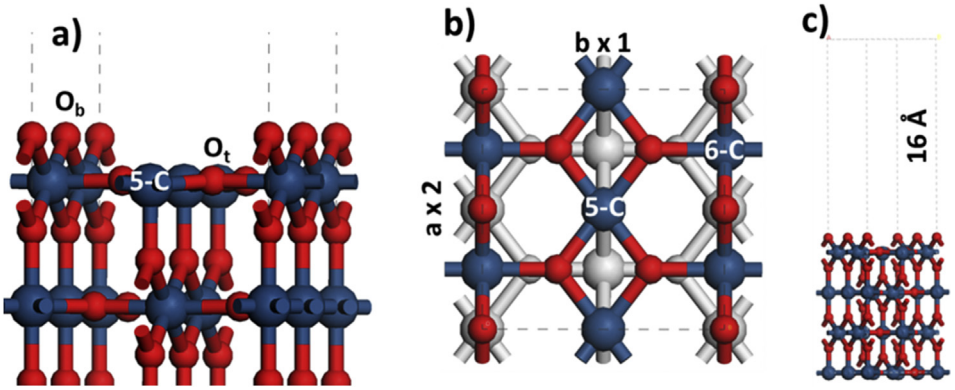

Fig. 1. Representation of the (110) MO_2 surface in the rutile phase: a) side view of the surface showing the oxygen bridging atoms (O_b), tri-coordinated oxygen (O_t) and the pentacoordinated metal site (5-C); b) top view of the surface (in color) showing the metal penta (5-C) and hexa-coordinated sites (6-C) and c) full view of the slab used for the calculations showing the space between slabs. Dotted lines represent the limits of the unit cell. (For interpretation of the references to color in this figure legend, the reader is referred to the web version of this article.)

Linear sweep voltammetry was used to determine the Tafel slopes for the individual electrocatalysts (Fig. 3). Tafel slopes are an indicator of electrocatalyst quality: the lower the Tafel slope, the faster the kinetics of the reaction and the more active the electrocatalyst (under constant electrocatalyst load conditions). Here we measured the electrocatalyst activity towards oxygen evolution as the desired electrode reaction. In acidic electrolyte, several possible reaction mechanisms of the OER have been proposed [17,18]. The Tafel slope cannot be used to directly identify the reaction pathway, but it may be used to determine the rate determining step in an assumed mechanism. However, this is not straightforward as the symmetry factor in the kinetic equations is usually not known and the considered value of 0.5 is not necessarily accurate under the experimental conditions [18]. Moreover, in the present case the electrocatalyst consist of agglomerates each of them probably having different reaction sites (SEM micrographs were obtained in a JEO, JSM-6490LV, in Supplementary information Fig. S2 shows the presence of agglomerates from 10 to 15 μm). Therefore, different rate-determining steps for different reaction sites can coexist and the measured Tafel slope then represents an average. The following reaction steps were generally proposed as the mechanism for the OER on anode electrocatalysts:

$$M + H_2O \rightarrow M{-}OH_{ads} + H^+ + e^- \quad (1)$$

$$M{-}OH_{ads} \rightarrow M{-}O_{ads} + H^+ + e^- \quad (2)$$

$$M{-}O_{ads} + M{-}O_{ads} \rightarrow 2M + O_2 \quad (3)$$

Here M represents an active site of the oxide electrocatalyst. OH_{ads} and O_{ads} represent adsorbed hydroxyl species and adsorbed oxygen atoms, respectively. A Tafel slope around of 120 mV dec^{-1} is generally attributed to the dissociative water adsorption with release of a proton and electron (Equation (1)) as rate determining step, whereas a value around 60 mV dec^{-1} suggests that the second step, Equation (2), is the rate determining step. The low Tafel slope can be attributed to the presence of adsorption intermediates involving OH species on the electrode surface. A possible contribution to the rate determining step from the electrochemical desorption of a proton from the adsorbed M–OH intermediate species at low current densities cannot be excluded.

The Tafel plots for the OER on $RuIrCoO_x$, RuO_2 and IrO_2 electrocatalyst surfaces are shown in Fig. 3. The Tafel slope data were subject to IR compensation (it was considered 10 Ω solution

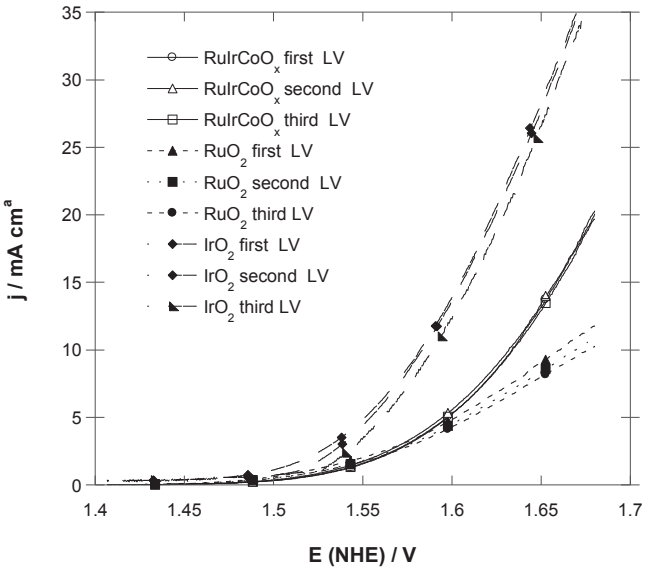

Fig. 2. Linear sweep voltammetry in anodic direction in 0.5 M H_2SO_4.

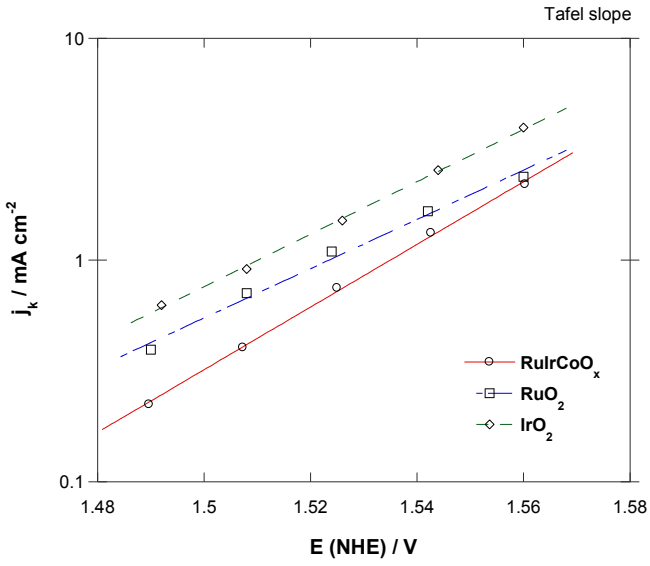

Fig. 3. Tafel plots for oxygen evolution reaction on $RuIrCoO_x$, RuO_2 and IrO_2 electrocatalysts in H_2SO_4 0.5 M.

Table 1
Tafel slope for oxygen evolution in H_2SO_4 0.5 M.

Catalyst	Tafel slope V dec^{-1}
RuO_2	0.090
IrO_2	0.085
$RuIrCoO_2$	0.068

resistance). Table 1 shows Tafel slopes analysis at low over potentials. At low over-potential current densities, the $RuIrCoO_x$ sample shows the lowest Tafel slope value, 0.068 V dec^{-1}, whereas RuO_2 and IrO_2 have Tafel slope values of 90 and 85 mV dec^{-1} respectively. Based on these results the rate determining step at low over-potentials is given by Equation (2).

A question arises naturally about the behavior of Co oxide alone in the presence of oxygen. De-Faria et al. [2] have reported a series of $RuO_2(x) + Co_3O_4(1 - x)$ compounds. The behavior of Co_3O_4 is completely different to that of the binary oxide mixtures, leading to higher Tafel slopes. The transformation to unstable CoO_2 and then to soluble CoO is possible at potentials higher than 1.47 eV. In agreement with our results, De Faria et al. experiments show that while dissolution is possible in pure Co oxide samples, the interaction with other oxides leads to a lower dissolution rate. Tüysüz et al. has recently reported the catalytic activity of a series of ordered mesoporous Co_3O_4 and composites in alkaline media showing a fairly good catalytic activity towards oxygen evolution which can be enhanced mainly with the addition of Cu during the synthesis [19].

3.2. Electronic density changes induced by Co as a dopant

First we focus on the changes in electronic structure when the surface is doped with Co, the formation of the doped compound has been proposed and its effect on oxygen evolution has been confirmed by different experimental and theoretical groups [2,20]. The effect of the addition of the dopant can be seen by analysis of the partial density of states (DOS). Metallic behavior of RuO_2 can be observed: from very low energy states up to ~−2 eV oxygen states are the main component of the total DOS, after that Ru states become predominant near the Fermi level (Fig. 4a). The presence of Co as dopant modifies the DOS of the surface, in both positions 5-coordinated (RuO_2-5D) and 6-coordinated (RuO_2-6D). The first leads to new states in a region near −2 eV in which no states were available, and the second creates more states near the Fermi level, occupied as well as unoccupied ones (Fig. 4b). Similar properties are observed for IrO_2 and its corresponding doped structures (not shown).

As the dopant atom has different size and electronegativity than the oxide atoms it is expected to cause differences in the charges of individual atoms and in general on the electron density of the surface. Electronic density accumulation/depletion graphs were calculated as the difference in electronic density of the pure and doped system in different sites. The graphs in Fig 5a and b shows electron density accumulation (blue)/depletion (red) in the plane *xy* plane directly on the surface of the slab. The Co atom presents electron density accumulation while causing electron density depletion in the next neighbor atoms. Since the size of Co atoms is smaller than the original Ru or Ir atoms, there is also electron depletion (red) in the region between Co and O atoms. Therefore differences in electronic partial charges of each of the atoms are expected. A quantitative analysis of the electronic density properties can be provided by Bader charge analysis [21], individual values of pristine and doped structures are shown in Table 2.

Bader charges of Pristine IrO_2 and RuO_2 are very similar, the charge of 6-coordinated atoms (3,4) is higher than those of 5-coordinated ones (1,2). When doped with Co, the Co charges are always less positive i.e. more electron density accumulated in Co. This higher electronic density induces a higher positive charge on Ru (2nd and 3rd highlighted columns) and Ir atoms (2nd and 3rd non highlighted columns) in comparison to the pure systems. The changes in electronic density for the doped systems confirm different chemical environments; therefore differences in reactivity are anticipated for the different sites comparing doped and un-doped cases.

3.3. Water adsorption and first oxidation stage

Water adsorption was simulated on top of all sites of doped and un-doped systems. The adsorption energy was calculated as the energy difference between the system containing the adsorbed water and those of separated water and slab systems. Adsorption energies and distances are reported in Table 3.

The adsorption energy is stronger on 5C sites in comparison to adsorption on 6C sites, independently of the surface and presence or absence or dopants; in some cases is even positive indicating a forbidden adsorption process, as it has been previously reported for different oxides [22]. Therefore, in the following, 6C sites are discarded as adsorption sites in the analysis of the OER mechanism. Adsorption of water on Ir-based surfaces is stronger than on Ru-based surfaces, independently of the site and doping position.

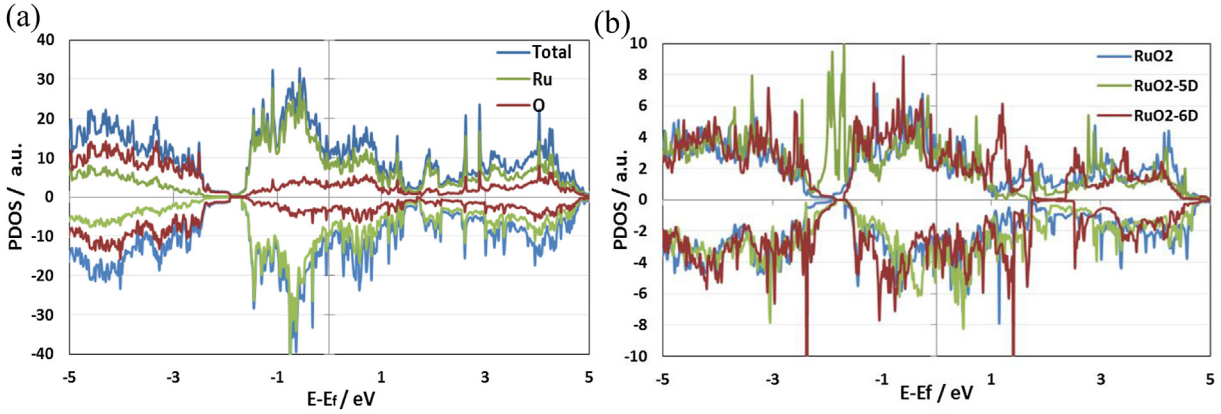

Fig. 4. Partial DOS of a) RuO_2 slab showing the contributions from O and Ru atoms; b) Surface partial DOS showing the differences when Co is added as a dopant in two different sites.

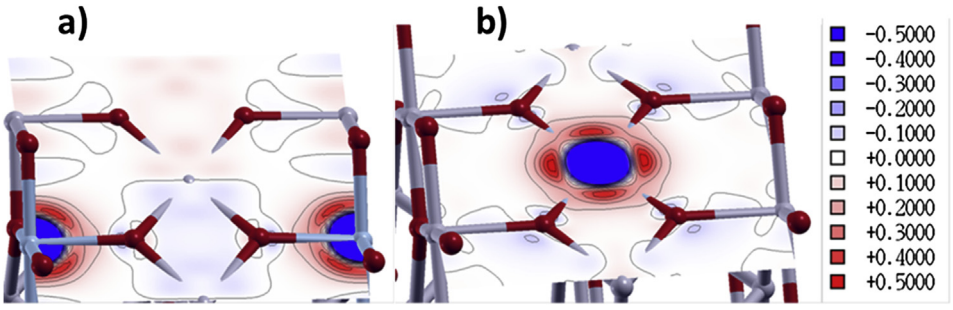

Fig. 5. Electronic density accumulation (blue)/depletion (red) on the surface plane of doped structures. Red, gray and light blue spheres represent O, Ru and Co atoms respectively. In b) the Co atom is located in the center of the figure. (For interpretation of the references to color in this figure legend, the reader is referred to the web version of this article.)

However, the presence of dopants influences the adsorption energy of water even if the adsorption is not directly on Co atoms. Compared to the undoped cases, water adsorption is stronger when the surface is doped in the M-6D site and adsorption is in a 5C site (−0.69 vs −0.61 eV in Ru based oxides). On the other hand when the surface is doped in the M-5D site and adsorption occurs in another 5C site the adsorption energy is slightly weaker (−0.56 vs −0.61 eV in Ru based oxides) than on the undoped surface. Bigger differences are found when the adsorption occurs directly on Co atoms. In this case, independently of Ru or Ir-based surface the adsorption of water is very weak. The differences in adsorption are related to the specific nature of the site affected by the Co atoms, therefore different hybridization and bond orders are expected. Fig. 6 shows the total electronic density in the plane along the O–M bond in three different water adsorption cases: on pure RuO_2, Ru-5D and Ru-6D structures. The electronic density shows different colors in the O–M bond area having a higher electronic density in the M-6D structure when adsorption is in the 5C site (Fig. 6b).

The proposed scheme of reaction for the breaking of the O–H bonds is shown in Fig. 7. Even if the process changes with the presence of the acid electrolyte and the effect of the electrochemical potential, the easiness for O–H breaking is well represented by this model and it leads to the analysis of the effect of the doping atom. Hydrogen evolution is neglected as it is assumed as being very fast in comparison to O evolution; therefore it is assumed that H leaves the surface in the form of protons leaving unaffected the main trends observed for oxygen evolution.

The reaction energy from water to OH + H is an indicative of the driving force for breaking the first O–H bond. Therefore doping RuO_2 and IrO_2 in the 6-coordinated site (M-6D) leads to a higher driving force for water splitting. On the other hand the direct adsorption of water on Co does not have a driving force for water splitting (purple lines) and is highly unlikely that the reaction may occur directly on Co atoms, because of both the weak adsorption energy and null driving force for O–H breaking. In the same analysis, the M-5D surfaces leads to a small decrease of the reaction energy; however in a real situation all sites will be present and the probability of the reaction occurring in each of them will determine the catalytic activity for the reaction.

For the calculation of transition states the climbing image nudged elastic band method (CINEB) was used [23]. For the undoped systems the activation barrier is null. As has been reported for other systems this step is easy and no activation energy or potential is needed. This behavior indicates that the breaking of the first O–H bond is not the rate-determining step. The adsorption energy directly on Co was the weakest and possibly no adsorption will be observed in this site. Following the same trend, the reaction energy is the lowest and consequently also the activation energy for this site is the highest (~0.2 eV) which however is still a very low activation energy. This gives a first indication that a direct reaction on Co atoms is prohibited but the influence of doping has an effect in neighboring sites allowing a higher driving force with no activation barrier. The barrier for O–H breaking was calculated on Pt and Au adatoms supported on TiO_2, the results indicated very different reaction barriers depending on the adatom nature [24]. In our case just analyzing adsorption and first stage dissociation would lead to a lower catalytic activity because of the small adsorption energy, high activation barrier and null driving force for O–H breaking directly on Co. Therefore we expanded the study in order to investigate the second O–H breaking.

3.4. OH adsorption and second oxidation stage

During the second stage of the OER, the OH formed during the first stage is transformed to an adsorbed O atom resulting from the O–H breaking. As in the first section we found out that water adsorption is less likely on 6-coordinated sites, therefore 6 coordinated sites were neglected and we only focus in adsorption on 5-coordinated sites.

OH adsorption energy is about three times stronger than water adsorption, this difference has been previously reported [25–27]

Table 2
Bader charges of surface *metal* atoms in pristine RuO_2 and IrO_2 and doped with Co in the 5-coordinated sites (5D) and 6-coordinated sites (6D). Only metal atoms are reported: 1 and 2 are five-coordinated atoms, 3 and 4 are six-coordinated atoms. Charges of Co atoms are underlined and in bold in each case, all other non-underlined data are Ir or Ru.

Metal atom	IrO_2	Ir 5D	Ir 6D	RuO_2	Ru 5D	Ru 6D
1	1.50	1.55	1.54	1.50	1.58	1.53
2	1.50	**1.33**	1.54	1.50	1.36	1.53
3	1.71	1.75	**1.40**	1.70	1.73	1.38
4	1.71	1.75	1.75	1.70	1.73	1.78

Table 3
Adsorption Energy of water (eV) on doped and un-doped sites of RuO_2 and IrO_2, Adsorption on Ru or Ir 5-coordinated and 6-coordinated sites (5C and 6C) and directly on Co (5C–Co and 6C–Co).

	Adsorption site			
Surface	5C (Ru or Ir)	5C–Co	6C (Ru or Ir)	6C–Co
RuO_2	−0.61		0.04	
Ru-6D	−0.69		−0.12	−0.02
Ru-5D	−0.56	−0.29	+0.07	
IrO_2	−1.02		−0.11	
Ir-6D	−1.06		−0.14	+0.1
Ir-5D	−1.01	−0.38	+0.22	

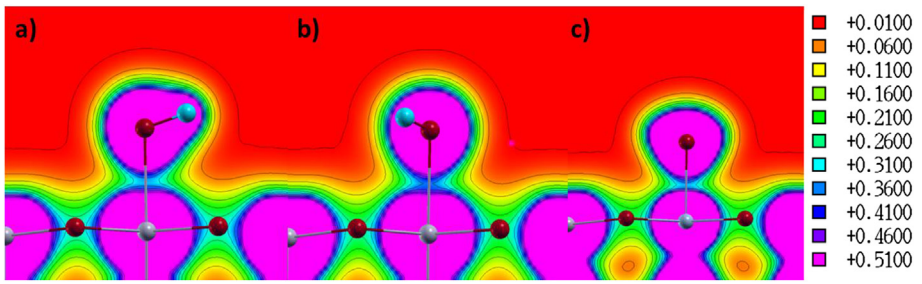

Fig. 6. Total electronic density along the O-M plane perpendicular to the surface. a) RuO_2 surface with water adsorbed in 6C site, b) Ru-6D with adsorption in 5C(Ru) and c) Ru-5D with water adsorption in 5C(Co). Scale is shown at right.

and has important consequences on the overall OER. Within the OER pathway, the adsorbed OH geometry is depicted in Fig. 8d. The OH adsorption behavior can be grouped in three different sets: the first includes structures where OH adsorption is done directly on Co atoms independently of the basic material being Ru or Ir oxide, the second group includes all structures where adsorption is done directly on Ru and the third where adsorption is on Ir sites. As in the case of water, the OH adsorption energy on Co sites is the weakest, so if water adsorption is weak, the formation of OH is even less likely which confirms that Co sites won't participate directly on the evolution reaction. For all sites containing Ru, independently of site, doping or without doping, the adsorption of OH is relatively the same; similarly for all Ir containing surfaces the OH adsorption is similar, but adsorption of OH is always stronger in Ir than in Ru-based surfaces. Therefore, differences in adsorption of OH only depend greatly on whether the adsorption is done directly on Co atoms or in the original Ru or Ir metal sites.

For the O–H bond breaking bigger differences are observed. There are surfaces that lead to an augment of the relative energy from O–H to O + H, i.e. formation energy of atomic O adsorbed on the surface is an endergonic process, while other configurations have a negative change in the relative energy, i.e. an exergonic process for O formation. Many materials present an endergonic reaction energy for O formation including pure oxides and doped structures when the adsorption is directly on Co; however for M-6D systems on both Ir and Ru oxides the process is exergonic, thus there is a driving force only in those structures that allow the formation of adsorbed oxygen. Therefore the effect of the dopant is more likely to be observed in this reduction step. As in the first step this particular structure (Co dopant on 6-coordinate site) presents advantages for the OER in comparison to the process on the pure oxides: 1) A more exergonic process for the breaking of the first O–H bond and 2) an exergonic process for breaking the second O–H bond.

The activation energy for O–H breaking depicted in Fig. 8-ii is higher than that observed in Fig. 7-ii; considering the exponential dependence of the kinetic parameters on activation energy, it clearly reveals a much more sluggish process. The highest activation barrier (0.56 eV) is observed on pure Ir oxide, which is also the structure with the highest adsorption energy. Thus, this higher adsorption energy could be responsible of the higher activation energy; on the other hand the activation energy on pure Ru oxide is only 0.39 eV with a weaker OH adsorption energy. By doping the oxides an effect on activation energies is also observed: doping Ir decreases the activation energy whether OH is adsorbed on Co or in Ir. But doping Ru has two opposite effects: doping on the M-6D site decreases the activation energy but when doping on the 5D site and

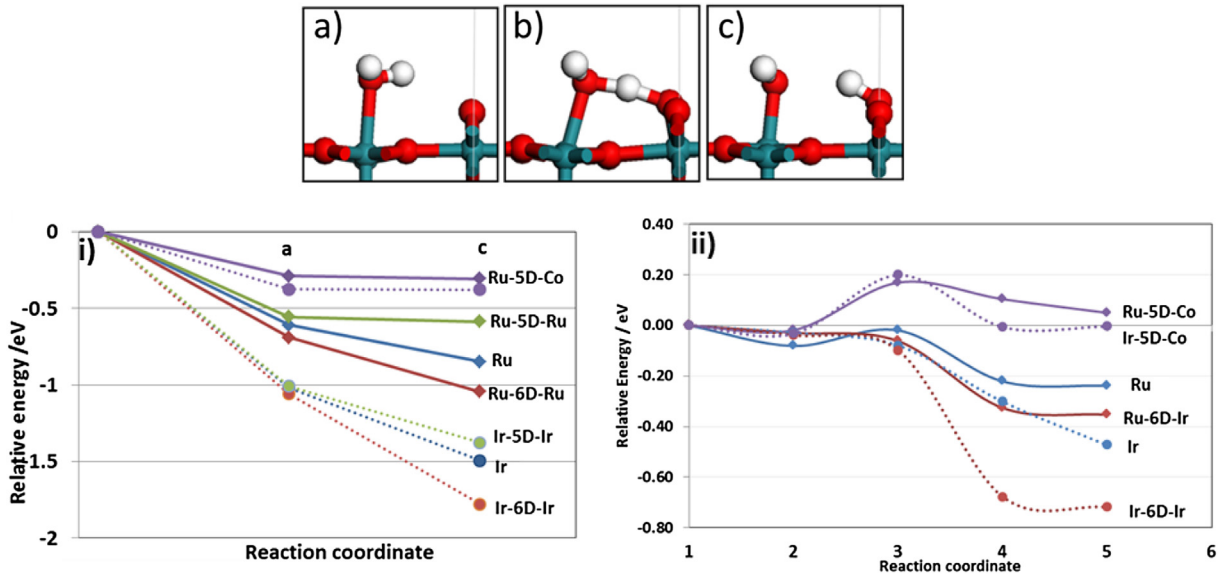

Fig. 7. Top: Reaction scheme for the first step of water splitting: a) Water adsorption, b) transition state, and c) formation of OH and H adsorbed. Bottom: i) Adsorption and reaction energy for O–H bond breaking and ii) CNEB calculations for the transition state connecting a and b. Lines are drawn to guide the eye, solid line for Ru-based and dotted line for Ir-based materials. M_1–xD–M_2 where M_1 is the metal base, x is the site where Co is present as dopant and M_2 is the metal where adsorption occurs.

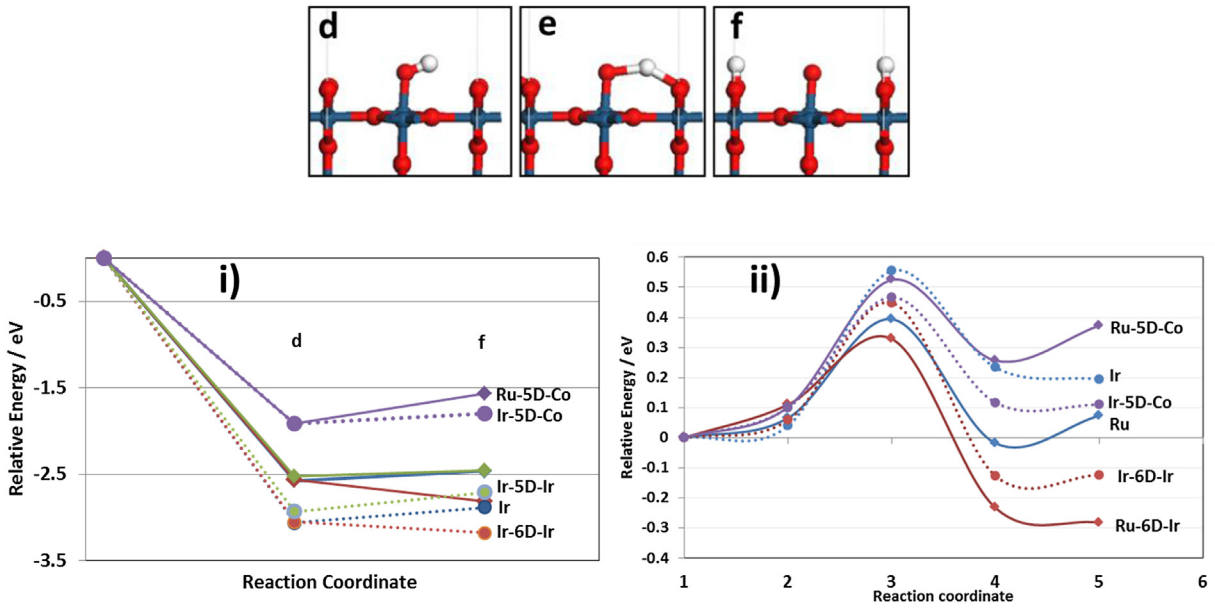

Fig. 8. Top: schematic representation of the second OER reduction step, Bottom: i) Adsorption and reaction energy for O–H breaking and ii) Activation energy for O–H breaking. In i) and ii) same line color represents same site, solid and dotted lines represent Ru and Ir-based surfaces respectively. M_1–xD–M_2 where M_1 is the metal base, x is the site where Co is present as dopant and M_2 is the metal where adsorption occurs.

adsorbed directly on Co the activation energy is higher although still lower than that on pure Ir. The effect of doping on the 6D site is observed again in this second step: the O–H reaction energy is endergonic and the activation energy for the same process is decreased.

4. Conclusions

Doping oxides presents a good opportunity to enhance the catalytic activity of electrolysis electrodes towards the OER, we have demonstrated that Co added as dopant in random surface sites during the synthesis has a significant effect on the electronic properties of the surface which leads to lower OER barriers and higher reaction driving force. Our complete description of the OER in doped Ru and Ir oxides using both experimental and theoretical simulations reveals that the $RuIrCoO_x$ catalyst is more stable in the reaction medium than RuO_2 and IrO_2 catalysts. A Tafel slope around 60 mV dec^{-1} for the $RuIrCoO_x$ suggests that the second H–O breaking is the rate determining step. The simulation of the process indicated that the second OH bond breaking has a higher barrier than the first one, and doping with Co allows higher driving force and smaller activation barrier, confirming that this is the rds. New opportunities can be found by allowing doping in specific sites, synthesizing specific structures and changing the dopant concentration and nature. Other transition metal dopants such as Ni, Cu, Cr, Fe, should be analyzed first theoretically in order to determine enhancement of the driving force for oxygen evolution and smaller barriers for O–H breaking. A trade-off in water and intermediates adsorption strengths is mandatory and can be analyzed by DFT simulations and then experimentally confirmed.

Acknowledgments

GRS acknowledges CONACYT for support this research with a postdoctoral fellowship. This work was partially supported by IPN multidisciplinary Project SIP-1540/2014 and by Secretaría de Ciencia, Tecnología, e Inovación del DF, SECITI DF, agreement ICYTDF/193/2012. Computational resources from Texas A&M Supercomputer facility, Texas A&M University Brazos HPC cluster, and Texas Advanced Computer Center (TACC) are greatly acknowledged.

Appendix A. Supplementary data

Supplementary data related to this article can be found at http://dx.doi.org/10.1016/j.jpowsour.2014.06.029.

References

[1] J.L. Corona-Guinto, L. Cardeno-Garcia, D.C. Martinez-Casillas, J.M. Sandoval-Pineda, P. Tamayo-Meza, R. Silva-Casarin, R.G. Gonzalez-Huerta, Int. J. Hydrogen Energy 38 (2013) 12667–12673.
[2] L.M. Da Silva, J.F.C. Boodts, L.A. De Faria, Electrochim. Acta 46 (2001) 1369–1375.
[3] J. Polonsky, I.M. Petrushina, E. Christensen, K. Bouzek, C.B. Prag, J.E.T. Andersen, N.J. Bjerrum, Int. J. Hydrogen Energy 37 (2012) 2173–2181.
[4] S. Song, H. Zhang, X. Ma, Z. Shao, R.T. Baker, B. Yi, Int. J. Hydrogen Energy 33 (2008) 4955–4961.
[5] A.J. Terezo, E.C. Pereira, Mater. Lett. 53 (2002) 339–345.
[6] C.P. De Pauli, S. Trasatti, J. Electroanal. Chem. 538 (2002) 145–151.
[7] J. Cheng, H. Zhang, H. Ma, H. Zhong, Y. Zou, Int. J. Hydrogen Energy 34 (2009) 6609–6624.
[8] K. Kadakia, M.K. Datta, O.I. Velikokhatnyi, P. Jampani, S.K. Park, P. Saha, J.A. Poston, A. Manivannan, P.N. Kumta, Int. J. Hydrogen Energy 37 (2012) 3001–3013.
[9] Y. Liang, Y. Li, H. Wang, J. Zhou, J. Wang, T. Regier, H. Dai, Nat. Mater. 10 (2011) 780–786.
[10] G. Kresse, J. Hafner, Phys. Rev. B 47 (1993) 558–561.
[11] G. Kresse, J. Furthmuller, Phys. Rev. B 54 (1996) 11169–11186.
[12] P.E. Blochl, Phys. Rev. B 50 (1994) 17953–17979.
[13] G. Kresse, D. Joubert, Phys. Rev. B 59 (1999) 1758–1775.
[14] K. Yang, J.J. Zheng, Y. Zhao, D.G. Truhlar, J. Chem. Phys. 132 (2010).
[15] C.-C. Wang, S.S. Siao, J.-C. Jiang, Langmuir 27 (2011) 14253–14259.
[16] H. Over, Chem. Rev. 112 (2012) 3356–3426.
[17] K. Kinoshita, Electrochemical Oxygen Technology, John Wiley, 1992.
[18] Y. Matsumoto, E. Sato, Mater. Chem. Phys. 14 (1986) 397–426.
[19] T. Grewe, X. Deng, C. Weidenthaler, F. Schueth, H. Tueysuez, Chem. Mater. 25 (2013) 4926–4935.
[20] V. Petrykin, K. Macounova, M. Okube, S. Mukerjee, P. Krtil, Catal. Today 202 (2013) 63–69.

[21] G. Henkelman, A. Arnaldsson, H. Jónsson, Comp. Mater. Sci. 36 (2006) 354–360.
[22] M. Garcia-Mota, A. Vojvodic, H. Metiu, I.C. Man, H.Y. Su, J. Rossmeisl, J.K. Norskov, ChemCatChem 3 (2011) 1607–1611.
[23] G. Henkelman, B.P. Uberuaga, H. Jonsson, J. Chem. Phys. 113 (2000) 9901–9904.
[24] S.-F. Peng, J.-J. Ho, Int. J. Hydrogen Energy 35 (2010) 1530–1536.
[25] M. Mavrikakis, J. Rempel, J. Greeley, L.B. Hansen, J.K. Norskov, J. Chem. Phys. 117 (2002) 6737–6744.
[26] J. Wirth, S. Monturet, T. Klamroth, P. Saalfrank, EPL 93 (2011) 6.
[27] J. Rossmeisl, Z.W. Qu, H. Zhu, G.J. Kroes, J.K. Norskov, J. Electroanal. Chem. 607 (2007) 83–89.